PRELIMINARY NUMERICAL ANALYSIS OF SELECTED PHENOMENA OCCURRING IN A RAIL FASTENING SYSTEM

Piotr Szurgott, Krzysztof Bernyś

Military University of Technology
Department of Mechanics and Applied Computer Science
Gen. Sylwestra Kaliskiego Street 2, 00-908 Warsaw, Poland
tel.: +48 22 6839941, fax: +48 22 6839355
e-mail: pszurgott@wat.edu.pl

Abstract

The results of numerical analysis of selected phenomena occurring in a rail fastening system were presented in the paper. The study is focused on assessment of the state of displacement and stresses in the rail pad subjected to a moving load. Two finite element models of the considered system were developed. The first one included elementary track segment corresponding to one sleeper. The second FE model consisted of several elementary segments. The number of the track segments was determined independently on the basis of dynamic analysis carried out using LS-DYNA computer code. Essential FE analyses were performed using MSC.Marc/Mentat software. FE model of the elementary segment included 600 mm length rail and a two-side shaped rail pad. The Mooney – Rivlin material model was applied for the polyurethane rail pad. The fastening systems were modelled using spring elements. The vertical and longitudinal spring elements were also applied for the ballast modelling. A case of moving load caused by single vertical force – one axle – was considered in the study. Methodology of moving load simulation in the MSC.Marc software was proposed. The obtained results allowed assessing the total deflection of the rail pad, the state of stress, the load distribution on respective sleepers. Moreover, they gave information about the behaviour of the rail pad under moving load in context of static test described in respective standards.

Keywords: rail pad, fastening system, moving load, numerical analysis, hyperelastic material

1. Introduction

Modern rail fastening systems consist of several components made of different materials to ensure optimal operating conditions for a railway superstructure – primarily its durability and reliability. Other aspects, such as noise reduction and travel comfort improvement, are also important and they are closely related to the fastener type. Elastic-damping properties of the railway surface may be discordant even for seemingly similar track sections. These properties may change during the operation as a result of wearing and tearing, a railway vehicle interaction, and an influence of the forces of nature. Several types of the fastening systems can be distinguished. The rail fastening systems have evolved for ages starting from the rail spikes. The next generations of the fasteners used screw spikes and bolt clamps. At present time, tension clamp fastening systems are applied more and more often.

Rail fastening systems play an important role in the railway infrastructure. Their main aim is to attach rails with the sleepers. Moreover, the fasteners reduce the dynamic effect of the rolling railway vehicle on the concrete sleeper and provide an electrical insulation between the rail foot and the sleeper as well.

The main aim of the study was to simulate the segment of the rail track, including fastening system, subjected to moving load. Obtained results allow characterising behaviour of the rail pad and other selected phenomena occurring in a rail fastening system under such load. The study is mainly focused on assessment of the state of displacement and stresses in the rail pad. Preliminary results of the analyses allow for overview of the interaction between respective components and they may be useful for further analyses and research of the rail fastening systems.

2. Description of the considered rail fastening system

Considered tension clamp fastening system consists of following components (Fig. 1a), [1]:

- pre-stressed concrete sleeper, type PS-94, lied on the crushed stone ballast,
- spheroidal iron anchor submerged in the sleeper,
- elastic rail pad between the sleeper and the rail foot,
- tension clamp attached to the anchor,
- insulator between the rail foot and the clamp toe,
- rail, type UIC 60.

Figure 1b presents the load – deflection characteristic of the tension clamp used in considered rail fastening system.

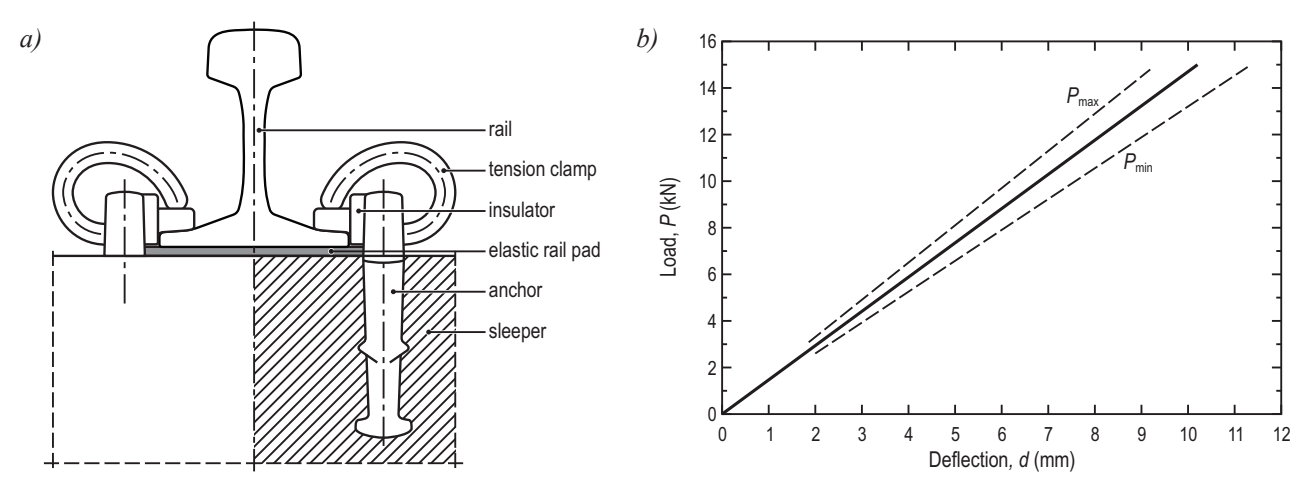


Fig. 1. Considered tension clamp fastening system (a) [1] and the load – deflection characteristic of the tension clamp

The elastic rail pad selected for the study is depicted in Fig. 2. It is not the actual object since it was developed as results of the quasi-optimisation analysis of carried out by Author [3]. Working area of the pad includes vertical cylindrical-shaped elements on both sides. Therefore, the pad is so-called two-sided rail pad. Overall thickness of the pad is 8 mm and the height ratio of cylindrical protrusions to the flat part equals 0.833. Proposed pad is made of polyurethane. Material properties were obtained from experimental test [2].



Fig. 2. CAD model of the two-sided rail pad selected for the study

3. Preliminary dynamic FE analysis

Preliminary dynamic analysis was performed in LS-DYNA computer code. It was aimed on the load distribution on successive sleepers. Results from the dynamic analysis allow determining number of the track segments for further simulations in MSC.Marc.

All necessary parameters and data for the dynamic analysis were taken from the Authors' previous studies focused on the bridge – track – train interaction, i.e. [4–6]. FE model of the test track (Fig. 3) included:

- 1. *Track* two parallel sets of beam elements. Rails were considered as prismatic beams deformable in flexure and shear, made of linearly viscoelastic material.
- 2. *Fastening systems* simulated using massless 1-D discrete non-linear spring and damper elements vertically oriented.
- 3. *Sleepers* placed in a distance of 0.6 m, modelled as elastic beams vibrating only vertically using beam finite elements and respective constraints, .
- 4. *Ballast* reflected by a set of vertical nonlinear spring and damper elements.
- 5. Sand-gravel mix layer and subsoil embankment modelled as a linearly viscoelastic material continuum.

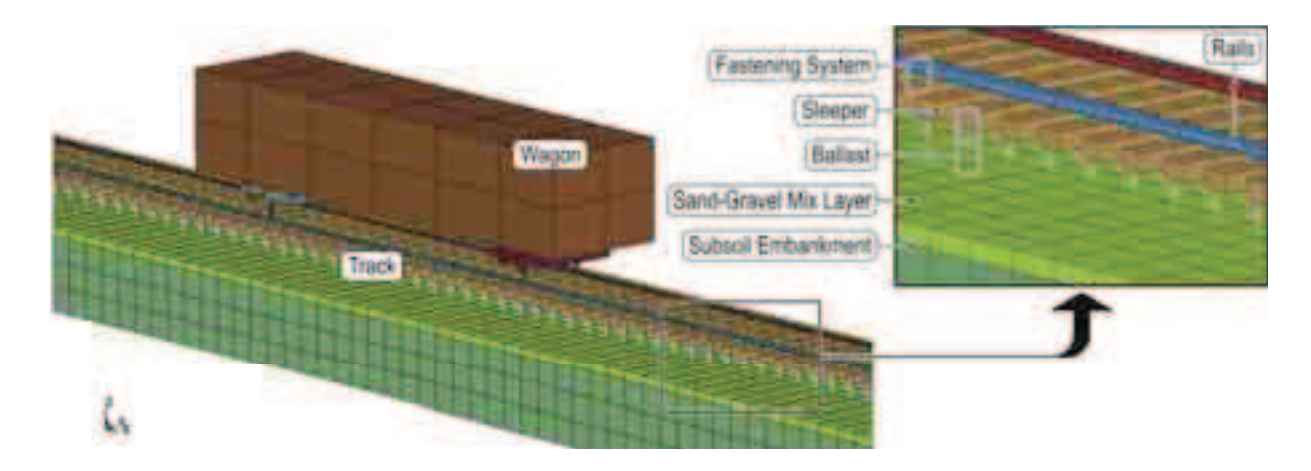


Fig. 3. FE model of the test track and wagon used in LS-DYNA dynamic analysis

RAIL_TRACK and RAIL_TRAIN modules available in LS-DYNA [7] were applied for approximate modelling the train – track interaction (without simulation of wheels' rotation). Simplified model of the platform wagon was developed. Considered wagon was equipped with two single axes instead of classic bogies. Therefore, its effect on the track could be treated as single-force load.

The maximum permissible static axle load – 22.5 kN – was taken into consideration. The wagon was moving at the speed of 10 m/s (36 km/h). Selected results of the dynamic analysis are presented in Fig. 4.

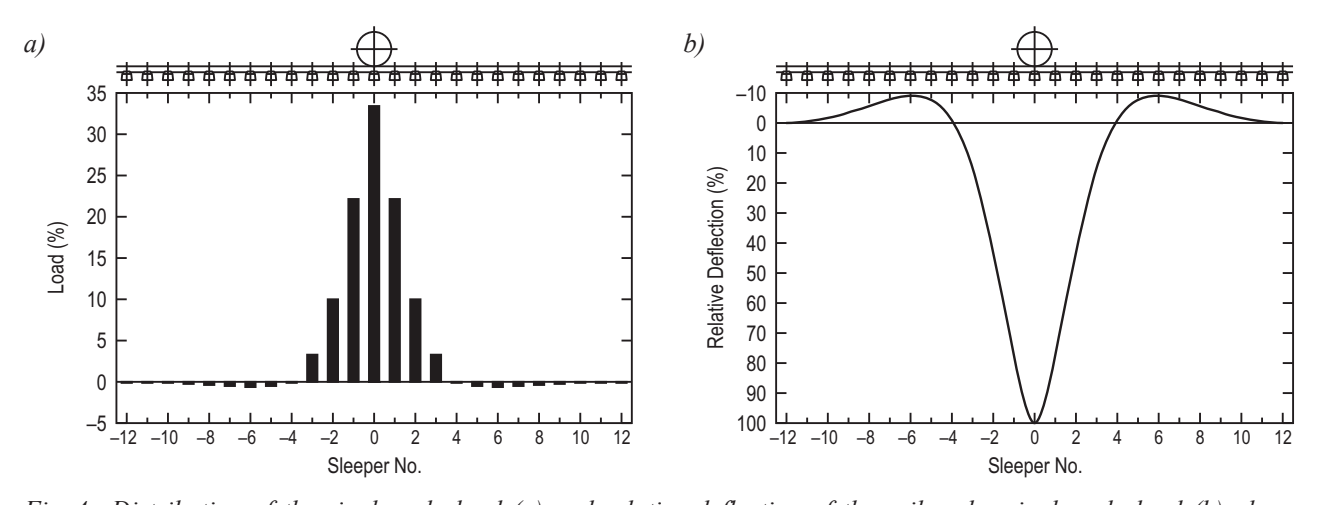


Fig. 4. Distribution of the single axle load (a) and relative deflection of the rail under single axle load (b) along successive sleepers

Maximum rail deflection and maximum load consequently appears under the axle. The maximum load equals about 33%. Behaviour of the rail is similar to results presented in [7], however load distribution along sleepers is few percent lower. The differences may be caused by different sleeper spacing and the assumed properties of the ballast and the subsoil embankment.

4. Quasi-dynamic FE analysis

Essential FE analysis was performed using MSC.Marc/Mentat software. FE model of the considered track included 12 sleepers and respective rail pads as well as 6600 mm length rail section (Fig. 5). Vertical symmetry of the system was assumed. Therefore a one rail could be simulated only. Ballast was modelled using one dimensional spring elements. Respective boundary conditions were applied for the system in transverse direction, whereas the movements of sleepers in vertical and longitudinal direction were possible. Constrains in longitudinal direction were used at both ends of the rail. Equivalent stiffness of the springs used to the ballast simulation was taken from the literature [8, 9] and provided in Tab. 1.

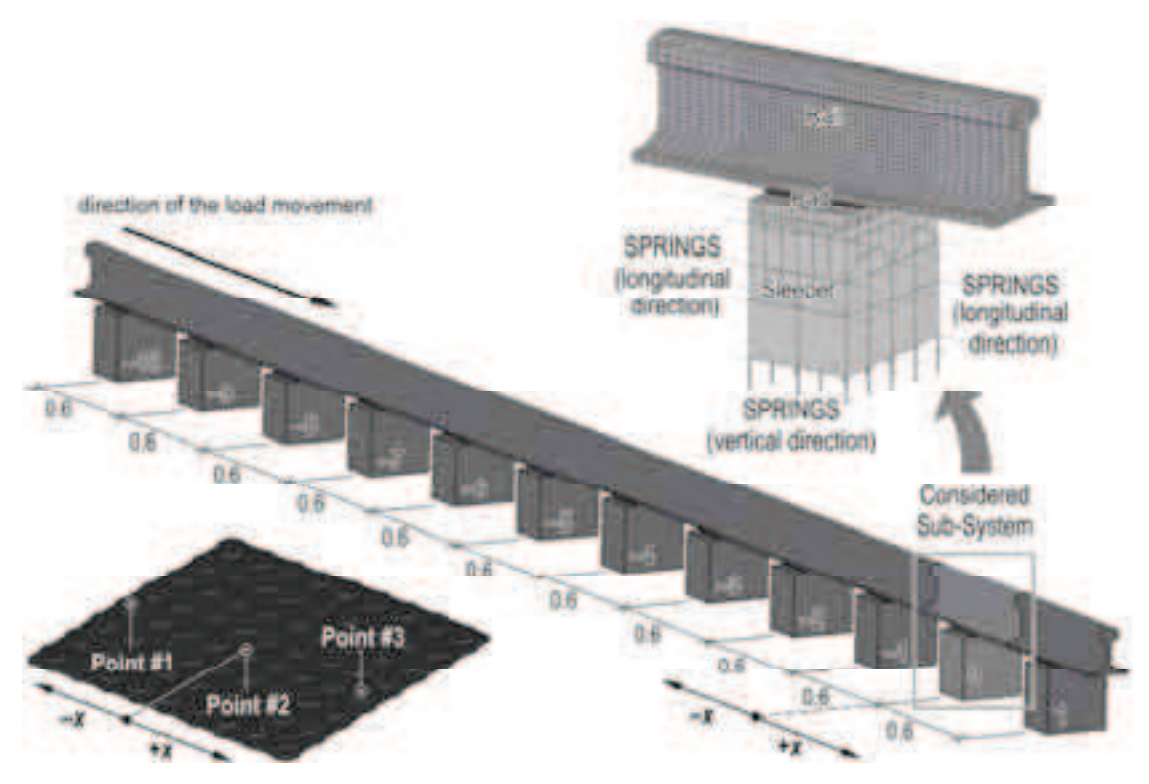


Fig. 5. FE model of the considered track used in MSC.Marc simulation – selected sub-system and three measurement points at the rail-pad protrusions are marked

Tab. 1. Vertical and longitudinal stiffness of the ballast [8, 9]

Vertical stiffness (kN/mm)	82 500
Longitudinal stiffness (N/mm)	11.8

Moving load – vertical force – was simulated in simplified way. The force P was applied in selected nodes located at the top of the rail head in the rail longitudinal symmetry plane. Force was changed during the analysis from zero to the maximum value and back to the zero, as depicted in Fig. 6. Therefore, the resultant force W was still constant and P equal throughout the analysis:

$$W = P_n + P_{n+1} = (1 - \alpha)P + \alpha P = P.$$
 (1)

Such approach allows for reflecting the moving load in static analysis.

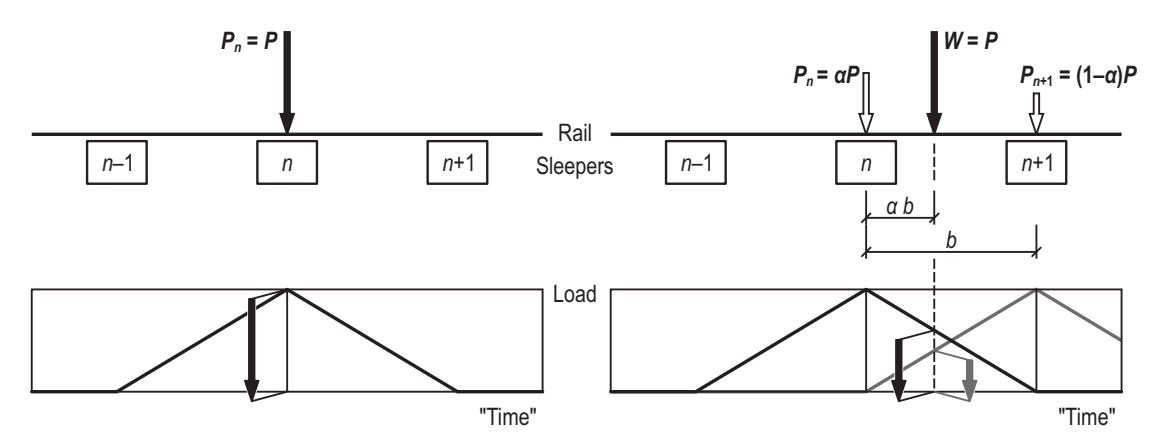


Fig. 6. Proposed method of the moving load implementation

Contact between respective components of the FE model was implemented in MSC.Mentat using contact table. The bilinear Coulomb type of friction was used in the current analysis. The friction coefficient between the sleeper and the pad was equal to 0.8, whereas between the pad and the rail foot -0.6.

The fastening clamp was modelled using one dimensional spring's jointed respective nodes in the rail foot and the insulator. Equivalent stiffness of each spring was calculated on the basis of the characteristic shown in Fig. 1b. In addition, the initial force option was implemented to simulated pre-compression of the rail – pad – sleeper system.

5. Material model

Considered rail pad was made of polyurethane. Material properties were determined based on experimental uniaxial compression and tension tests [2]. Numerical analysis was carried out using the MSC.Marc software which includes a module for modelling high-elastic materials. The Mooney – Rivlin group of material models were selected in this case. They were based on the deformation energy function *W* that can be written in the following polynomial form [10]:

$$W = \sum_{i+j=1}^{n} C_{ij} (I_1 - 3)^i (I_2 - 3)^j,$$
(2)

where I_1 and I_2 are deformation invariants, and C_{ij} are constants defined for a particular material. The deformation invariants are given as follows:

$$I_1 = \lambda_1^2 + \lambda_2^2 + \lambda_3^2$$
, and $I_2 = \lambda_1^2 \lambda_2^2 + \lambda_2^2 \lambda_3^2 + \lambda_3^2 \lambda_1^2$, (3)

where λ_1 , λ_2 , λ_3 are elongations of the element under consideration along particular directions, as depicted in Fig. 7a.

Determination of the C_{ij} constants expressed in (2) was performed using Experimental Data Fitting algorithm included in MSC.Mentant preprocessor. It was based on the method of least squares [6]. The 2-parameter Mooney – Rivlin model with C_{10} and C_{01} constants was assumed for analysis. The deformation energy function W for a selected material model is given as follows:

$$W = C_{10}(I_1 - 3) + C_{01}(I_2 - 3). (4)$$

Assuming an incompressibility of the material the deformation energy W can be written in the following form:

$$W = C_{10} \left(\lambda_1^2 + \frac{2}{\lambda_1} - 3 \right) + C_{01} \left(2\lambda_1 + \frac{1}{\lambda_1^2} - 3 \right), \tag{5}$$

or

$$W = C_{10} \left((1 + \varepsilon_1)^2 + \frac{2}{1 + \varepsilon_1} - 3 \right) + C_{01} \left(2 (1 + \varepsilon_1) + \frac{1}{(1 + \varepsilon_1)^2} - 3 \right). \tag{6}$$

Having defined the deformation energy W, one can determine the stress components along the directions of interest as partial derivatives:

$$\sigma_{1}(\varepsilon_{1}) = \frac{\partial W}{\partial \varepsilon_{1}} = 2 \left[C_{10} \left((1 + \varepsilon_{1}) - \frac{1}{(1 + \varepsilon_{1})^{2}} \right) + C_{01} \left(1 - \frac{1}{(1 + \varepsilon_{1})^{3}} \right) \right]. \tag{7}$$

The above relation is the stress – strain characteristic of the polyurethane under consideration. The results of the experimental test were approximated by the stress – strain curve for the constant value $C_{10} = 1.5218$ MPa and $C_{01} = 1.5139$ MPa (Fig. 7b).

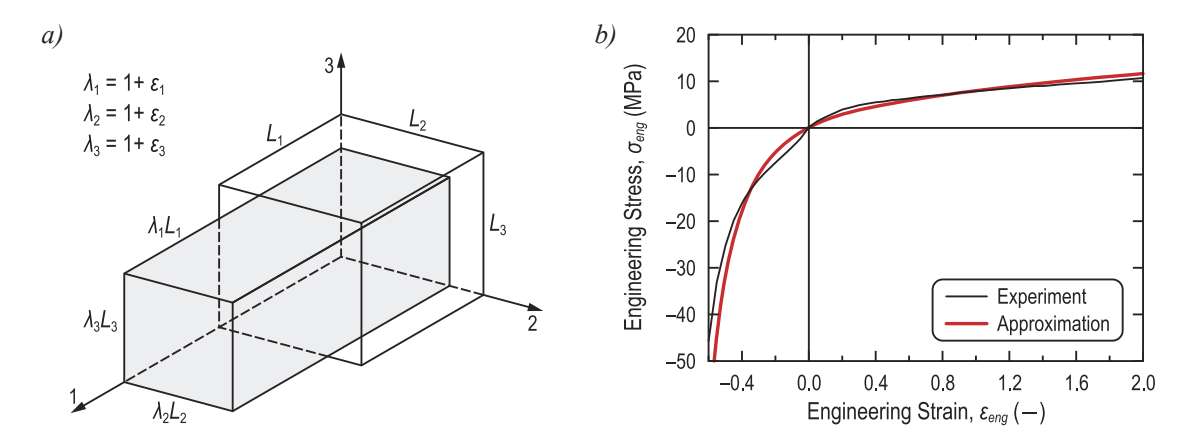


Fig. 7. Elongations λ_1 , λ_2 , λ_3 of the element under consideration in the case of uniaxial tension (a) [11]. Approximation of the experimental test results by 2-parameter Mooney – Rivlin material models (b) [2]

6. Results of the quasi-dynamic FE analysis

Figure 8a shows changes in the equivalent stress σ_{red} for the considered rail-pad (marked in Fig. 5) as a function of the moving load coordinate x. Presented values are the highest stresses obtained in the whole pad FE model for each time step. Maximum values appear once the load is located exactly over the considered sub-system (x = 0). They are about three times higher than those obtained for the pre-compressed system only. The graph depicted for the positive x coordinates was reflected since the FE model of the track was limited to 6,600 mm. Such assumption does not result in significant errors in presented diagram. Similar results were obtained for the vertical stress component σ_z (Fig. 8b). The rail-pad is compressed due to pre-compression of the system as well as the load moving over the rail. Maximum increase in stress caused by travelling rail-way vehicle is about three times higher than for the pre-compressed system.

Figure 9 presents contours of the equivalent stress σ_{red} and the vertical displacement for the considered rail-pad while the load is located exactly over the pad. A quarter of the numerical FE model is shown to better visualize of the stress distribution in respective cross-sections of the object.

Relative vertical displacements of three selected points located on the pad's protrusions (Fig. 5) are depicted in Fig. 10. "Relative" in this case is defined as the displacement of the FE model node without considering vertical displacement of the sleeper. Differences in displacement in the centre section of the diagrams are related to the load movement. However, they can be considered also as a boundary effect due to simplification of the model. Nevertheless, the differences are rather slight. Hence, it can be assumed that rail-pad under moving load is compressed and both compressing surfaces – rail foot bottom face and the sleeper upper face – are parallel. An influence of the rail bending between successive sleepers on the pad behaviour can be omitted.

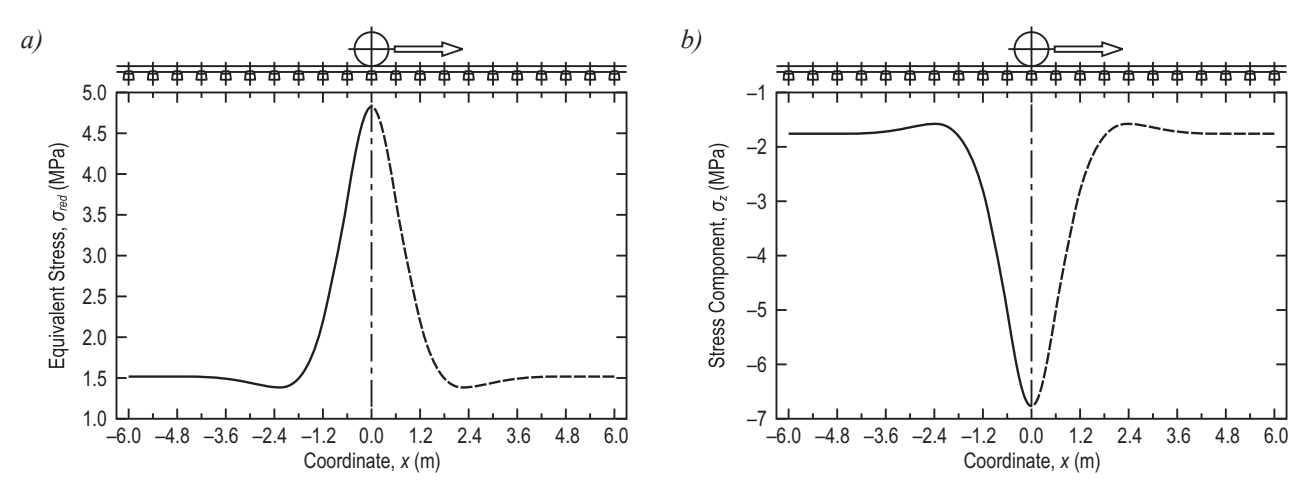


Fig. 9. Equivalent stress σ_{red} (a) and vertical stress component σ_z (b) vs. moving load coordinate x for the rail-pad

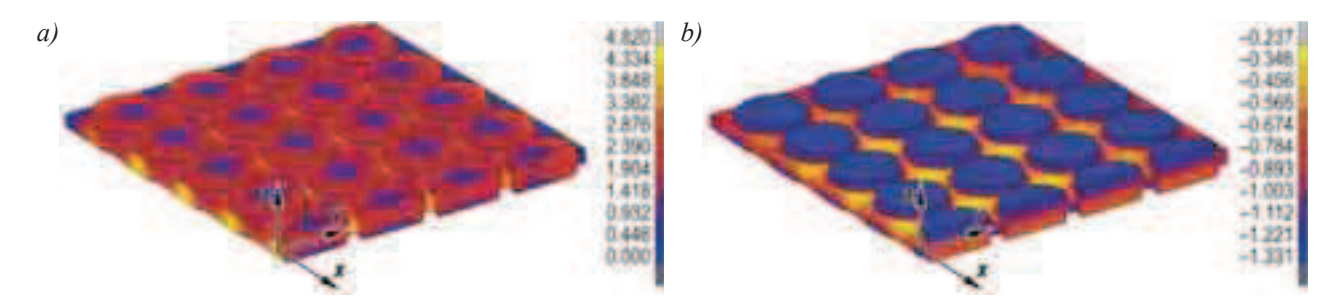


Fig. 10. Contours of the equivalent stress σ_{red} (a) and vertical displacement d_z (b) for the maximum loaded rail-pad

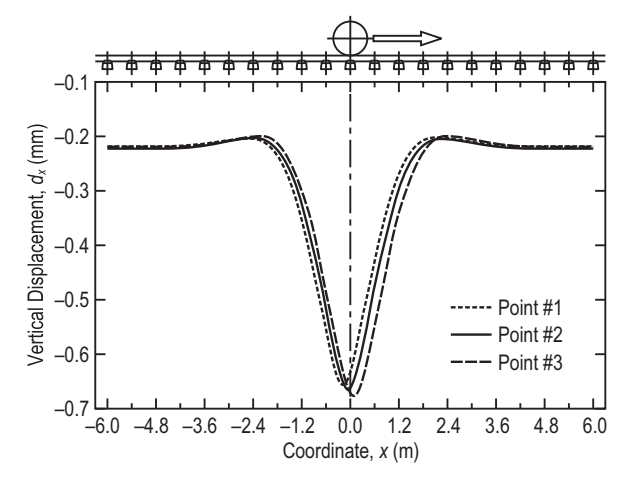


Fig. 10. Vertical displacement of selected points #1, #2, #3 located on the pad protrusions

Conclusions

The preliminary study presented in the paper was focused on assessment of the state of displacement and stresses in the polyurethane rail pad subjected to a moving load. According to obtained results it can be concluded that increase in stress caused by maximum permitted load is about three times higher than for the pre-compressed system only. This conclusion could not be generalized since it concerns the specific rail fastening system with the strictly defined distance between successive sleepers. However, due to proposed simulations the effect of the moving load can be determined in a qualitative way. Moreover, the influence of the rail bending on the pad behaviour while the load is located between sleepers is inconsiderable. It can be assumes that the rail pad is subjected to the vertical compression load only. This conclusion is consistent with the standards of the static test for rail fastening system that considered the load perpendicular to the rail foot mostly.

References

- [1] Oczykowski, A., Research and Development of the SB Tension Clamp Fastening System, Railway Problems, No. 150, pp. 121–156, 2010 [in Polish].
- [2] Szurgott, P., Gotowicki, P., Niezgoda, T., *Numerical Analysis of a Shaped Rail Pad Under Selected Static Load*, Journal of KONES Powertrain and Transport, Vol. 19, No. 1, pp. 407–414, 2012.
- [3] Numerical FE Analysis of Rail Pads in the Rail Fastening System, Final Raport, No. PBN/03-500/2010/WAT, Military University of Technology, Warsaw, Poland 2010.
- [4] Szurgott, P., Klasztorny, M., Grosel, J., Wójcicki, Z., *Experimental Validation of Numerical Modelling of the Bridge Track Moving Train System*, WIT Transactions on Modelling and Simulation, Vol. 51, pp. 97–109, 2011.
- [5] Klasztorny, M., Szurgott, P., *Modelling and Simulation of Bridge Track Train Systems at High Service Velocities with LS-DYNA*®, 12th International LS-DYNA Users Conference, Dearborn, MI, United Staes, 2012.
- [6] Szurgott, P., Klasztorny, M., Niezgoda, T., Modelling and Numerical Simulation of Symmetric Vibrations of the KNI 140070 Viaduct Ballasted Track KTX Train System, Journal of KONES Powertrain and Transport, Vol. 17, No. 3, pp. 415–422, 2010.
- [7] Profillidis, V. A., *Railway Management and Engineering*, 3rd Edition, Ashgate Publishing Ltd., England 2006.
- [8] Klasztorny, M., *Dynamics of Beam Bridges Loaded by High-Speed Trains* [in Polish], WNT, Warsaw, Poland 2005.
- [9] Friszman, M. A., Railway Track and Its Interaction with the Rail Vehicles [in Polish], WKiŁ, Warsaw 1983.
- [10] Marc 2007 r1, Volume A: Theory and User Information, MSC.Software Corporation, United States 2007.
- [11] Szurgott, P., Boczkowska, A., Kurzydłowski, K. J., Niezgoda, T., *Numerical Strength Analysis of Magnetic Fields Interaction with Elastomer Materials Containing Iron Particles*, Proceeding of the III ECCOMAS Thematic Conference on Smart Structures and Materials, Gdansk, Poland 2007.